Pergamon

SCIENCE DIRECT®

Tetrahedron 59 (2003) 6301–6309

TETRAHEDRON

Theoretical study on the polymerization mechanism of substituted maleimides by using a chiral catalyst with Zn^{2+}

Kenzi Hori,* Kazuaki Yoshimura, Hidetoshi Ohno,† Kenjiro Onimura and Tsutomu Oishi

Department of Applied Chemistry and Chemical Engineering, Faculty of Engineering, Yamaguchi University, Tokiwadai, Ube 755-8611, Japan

Received 21 May 2003; accepted 23 June 2003

Abstract—It is possible to synthesize poly(N-substituted maleimide) by using a chiral complex consisting of a zinc and *N*-diphenylmethyl-1-benzyl-2-pyrrolidinoethanamine (DPhBP). The optical specific rotations $[\alpha]_{435}^{25}$ in obtained polymers depend on the chirality of ligands in the catalysts. In the present study, density functional theory (DFT) calculations were adopted to investigate the polymerization mechanism in detail. The bulky diphenylmethyl group in the chiral ligand is effective to enhance the formation of the product in the initiation reaction. The geometry related to the pyrrolidine ring of the chiral ligand in the Zn catalyst is responsible for determining the configuration of polymers. It was also confirmed that the bulky substituent on the N atom of the N-substituted maleimide is another factor for obtaining polymers with high $[\alpha]_{435}^{25}$.

1. Introduction

Much attention has been focused on synthesizing polymers with optical activity.[1] It is because such polymers, which are adsorbed on or chemically bonded with silica gels, can distinguish chirality of small molecules in order to separate racemic products from organic syntheses.[2] These polymers can be used as chiral stationary phases of high pressure liquid chromatograph. Chirality was added to polymers for their biological decomposition and the mechanism has been investigated.[3]

N-Substituted maleimide (RMI) has two prochiral carbons so that its polymer has substantially chiral carbons in the main chain. The optical property of the RMI polymers depends on the *R*/*S* ratios of the main chain carbons as well

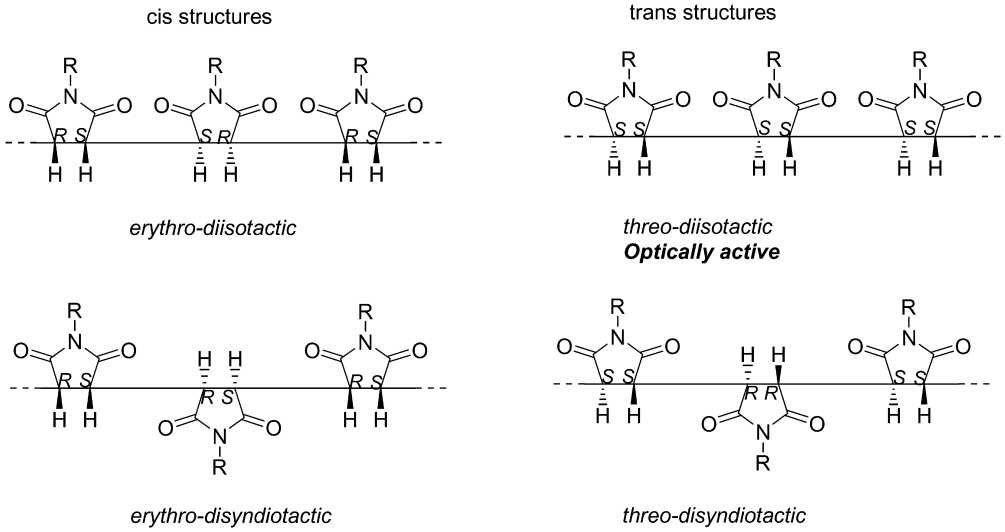

Scheme 1.

Keywords: polymerization; chiral ligand; density functional theory.
* Corresponding author. Tel.: +81-836-35-9045; fax: +81-836-35-9933; e-mail: kenji@sparklx.chem.yamaguchi-u.ac.jp
† Also at: Materials & Chemicals Research Laboratory, Idemitsu Petrochemical Co. Ltd., 1-1 Shingu-cho, Shunan 745-8691, Japan.

0040–4020/$ - see front matter © 2003 Elsevier Ltd. All rights reserved.
doi:10.1016/S0040-4020(03)01014-7

Table 1. Physical parameters of poly(CHMI) in experiments by using DPhBP or (*S*,*S*)-Bnbox as the chiral ligand in the catalysts

Run	Initiator	Yield (%)	10^{-3} (M_n)[a]	M_w/M_n[a]	$[\alpha]^{25}_{435}$ (°)[b]
1	FlLi–DPhBP	71	2.33	1.83	−8.2
2	Et_2Zn–DPhBP	78	2.01	2.13	−155.3
3	BuLi–(*S*,*S*)-Bnbox	97	4.1	2.36	111.4
4	Et_2Zn–Bnbox	99	8.1	3.25	117.5

[a] By use of GPC.
[b] c=1.0 g dL^{-1}, THF (runs 1 and 2), $CHCl_3$ (runs 3 and 4).

as existence of helixes. Scheme 1 shows four types of the polymer main chain geometry which is dependent on the mechanism of polymerization. The RMI polymerization via *cis* addition produces *erythro*-diisotatctic or *erythro*-disyndiotactic polymers which are not optically active.[4] As chiral stereogenic centers, (*R*,*R*) or (*S*,*S*) configurations, continue alternatively in *threo*-disyndiotactic polymers, this polymer is not optically active, either. On the other hand, one of the configurations only exists in the main chain carbons of *threo*-diisotactic polymers and such polymers are optically active. Even though all the carbons in a poly(RMI) do not have the same configuration, the polymer with excess amount of chiral carbons with (*R*,*R*) or (*S*,*S*) configurations results in being optically active.

Oishi and his co-workers have synthesized many optically active polymers[5] by using the technique that RMIs were polymerized with catalysts consisting of a chiral ligand and a metal ion such as Li^+ and Zn^{2+} (Scheme 2).[6] The magnitude of the specific optical rotation at 25°C, $[\alpha]^{25}_{435}$, in poly(RMI)s depends not only on the metal ion but also on the chiral ligand in the catalysts as shown in Table 1. While BuLi–(*S*,*S*)-Bnbox, a Li^+ complex with 2,2′-ethylpropylidene-((4*S*)-4-benzyl-2-oxazoline), catalyzed formation of polymers with a high $[\alpha]^{25}_{435}$, as high as 111.4°, the Et_2Zn–Bnbox complex is also effective for producing such polymers, $[\alpha]^{25}_{435}$=117.5°. It was confirmed that RMI-polymers with a positive $[\alpha]^{25}_{435}$ include (*S*,*S*)-configuration more than (*R*,*R*)-configuration carbons in the main chain.[7] FlLi–DPhBP (Fl: fluorene, DPhBP: *N*-diphenylmethyl-1-benzyl-2-pyrrolidinoethanamine) made polymers with a low optical activity, $[\alpha]^{25}_{435}$=−8.2°. The Et_2Zn–(*S*,*S*)–DPhBP complex was, however, the most effective to synthesize polymers with the high $[\alpha]^{25}_{435}$=−155.3°. As will be discussed later, the metal of Zn^{2+}–DPhBP catalyst has an empty site which can accept a RMI for polymerization. A similar coordination environment is expected for the Li–DPhBP complex. The combination of the metal ions and the chiral ligands in the catalysts is responsible for the optical property of polymers obtained. ^{13}C NMR experiments showed that ratios of *threo*-diisotactic structures in polymers increase with the increase in the absolute value of $[\alpha]^{25}_{435}$ even though such polymers also include main chain carbons with the other three configurations.[8]

We investigated the polymerization mechanism of RMI for a catalysis of Bnbox with an alkyl lithium since details of the polymerization mechanism of RMIs have not been understood.[9] It was confirmed that the initiation reaction determines the optical property of the polymers using the Li–Bnbox catalyst. Although the geometry of the chiral ligand plays an important role in determining the configuration of the main chain carbons in the product of the initiation reaction, it has little effects on the *R*/*S* selectivity for propagation reactions. It is, therefore, very interesting to investigate and compare difference of mechanisms between polymerizations using Li–Bnbox and the Et_2Zn–DPhBP complexes. In the present study, the polymerization mechanism of RMIs with DPhBP model complexes with Zn^{2+} was investigated by use of density functional theory (DFT) calculations.

2. Method of calculations

DFT calculations were adopted to investigate the polymerization mechanism of RMI by using the catalyst, the alkyl Zn-complex **2** with methyl-(1*S*-methyl-2-pyrrolidin-1-yl-ethyl)-amine and its derivative with an *N*-diphenylmethyl group. For the simplicity of calculations, HMI (maleimide) was mainly used as a monomer. We used the Gaussian 98 program for the DFT calculations.[10] All the transition states (TS), reactants and products were optimized at the B3LYP/LANL2DZ[11] level of theory. Complexes with the diphenylmethyl group in the catalyst are too large to perform detailed analysis of the reactions at the same level of theory, we adopted the integrated molecular orbital+molecular orbital (IMOMO) method developed by Morokuma et al.[12] While the LANL2DZ basis sets were used for optimizations of molecules without substituents, the ONIOM(B3LYP/LANL2DZ/B3LYP/LANL2MB) level of theory was used for investigating reactions of the catalyst with the bulky group. In these calculations, two phenyl groups were treated as the low layer for geometry optimizations.

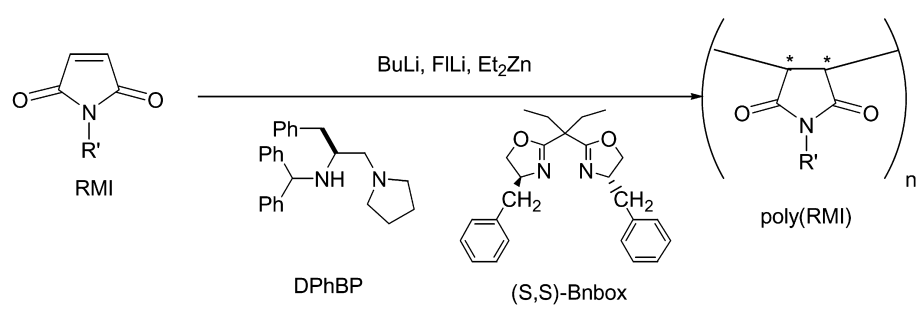

Scheme 2.

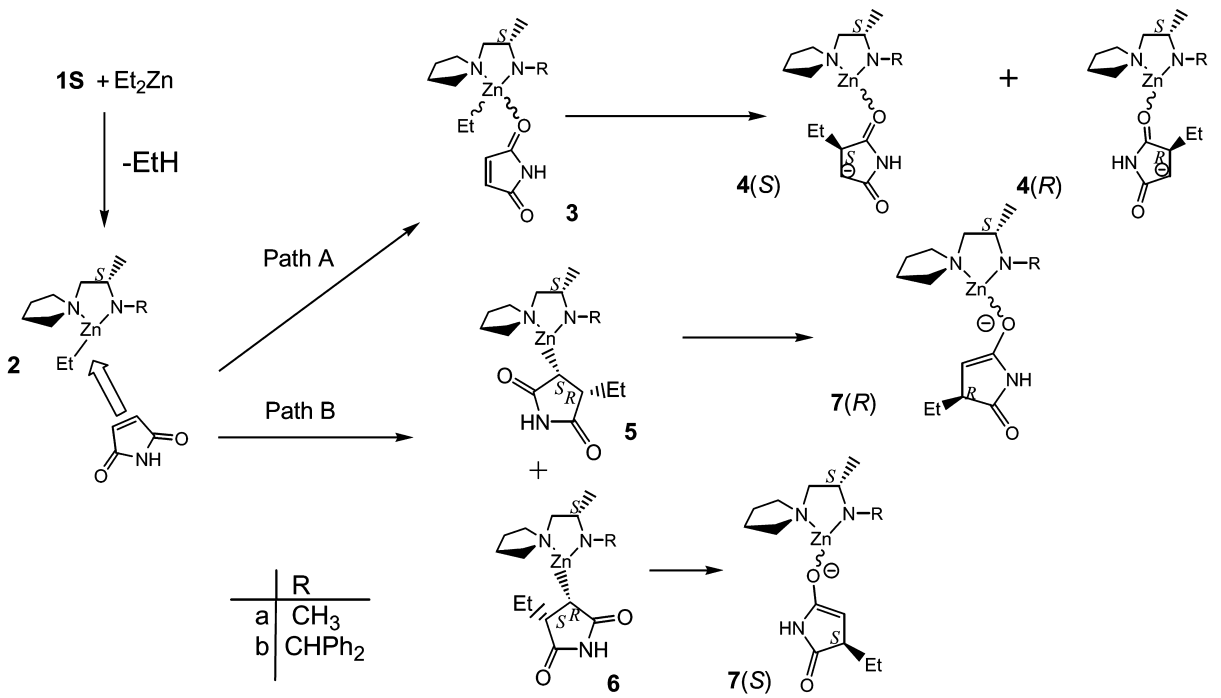

Scheme 3.

In analyzing propagation reaction mechanisms, all the geometries including TS structures were optimized at the RHF/LANL2DZ level of theory and B3LYP/LANL2DZ//RHF/LANL2DZ energies were calculated in order to obtain better energy description among TSs of the reactions.

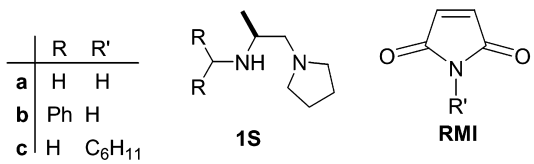

3. Results and discussions

3.1. Mechanisms of the initiation reaction

It is necessary that Et_2Zn reacts with **1S** (**1** with the chiral carbon of the *S*-configuration) to form ethane and the catalyst **2** with an empty coordination site for polymerization at the beginning of the initiation reaction as shown in Scheme 3. No solvents can coordinate to the empty site of Zn^{2+} in toluene, the solvent used in experiments. There are two candidates for mechanisms of the initiation reaction.[‡] One is Path A where an HMI coordinates to the Zn^{2+} to form **3**, followed by a transfer of the ethyl group from Zn^{2+} to the coordinated HMI. As HMI has an enantiotopic face, the difference in the ethyl group position on the five-membered ring results in producing two isomers, **4**(*S*) or **4**(*R*) in which they have a carbon with *S* or *R* configuration in the ring, respectively. The other is Path B in which the transfer of the ethyl group proceeds without coordination of the HMI to Zn^{2+}. The plausible products are **5** and **6**. They have anionic carbons which coordinate to Zn^{2+}. It is likely that they change their coordination atom to form **7**(*R*) and **7**(*S*), in which the enolate oxygen coordinates to Zn^{2+} since the enolate oxygens are more negative than the anionic carbons. Figure 1 displays the energy diagram among molecules in Scheme 3. We could obtain no TS structures which lead to form intermediates with the ethyl group on the RMI carbon distant from Zn^{2+}.

The reaction via Path A proceeds after **3** forms and this step turned out to be endothermic by 8.8 kcal mol^{-1}. It was confirmed that the ethyl group moves to the olefinic carbon close to Zn^{2+} and the group can select one of two possible planes of HMI such as **4a**(TS,*R*) and **4a**(TS,*S*). Therefore, the coordination geometry of HMI determines which product with *R* or *S* configuration is obtained.

In **4a**(TS,*R*), the ethyl group occupies the position between Zn^{2+} and HMI. As the Zn^{2+}–O length was calculated to be 2.064 Å, a carbonyl oxygen of HMI coordinates to the metal during the reaction. This feature in geometry on the TS of Path A stabilizes by 5–8 kcal mol^{-1} in comparison with those of Path B. **4a**(TS,*R*) turned out to be more stable by 2.0 kcal mol^{-1} than **4a**(TS,*S*).

The carbonyl oxygen cannot interact with Zn^{2+} during the initiation reaction via Path B. Zn–C distances in **6a**(TS) were calculated to be 2.302 and 2.323 Å, respectively. This feature in geometry shows that forming the Zn–C(HMI) bond and breaking the Zn–C(Et) bond proceed simultaneously. Activation energies were 25.4 and 22.5 kcal mol^{-1} for **5a**(TS) and **6a**(TS). The intermediates of Path B, **5a** and **6a** have the anionic carbons coordinating to Zn^{2+}. It is possible to consider their geometrical isomers

[‡] We could optimize no Zn^{2+} complexes with five ligands with a trigonal bipyramid geometry. Therefore, we did not consider any mechanisms via complexes with the geometry.

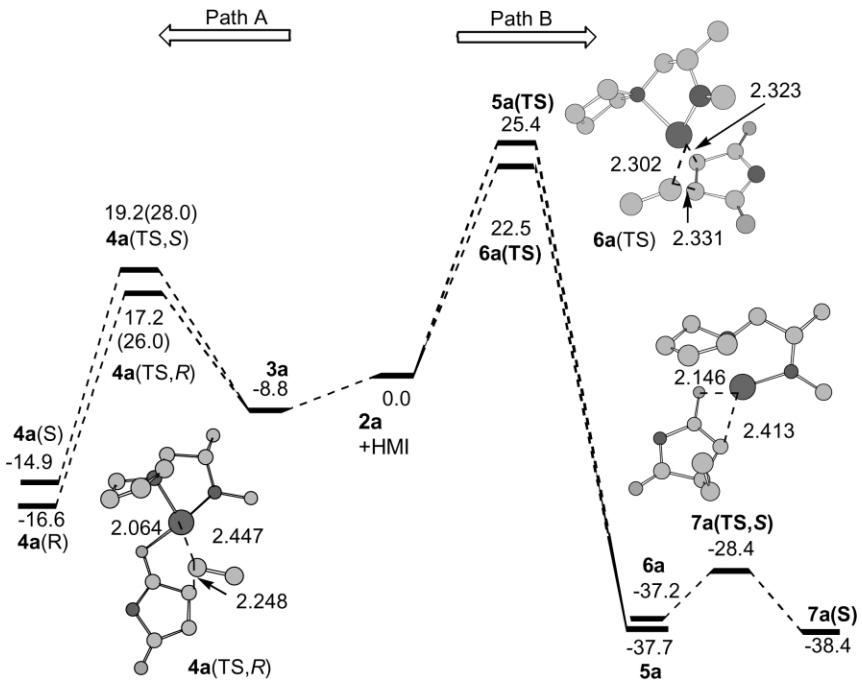

Figure 1. Energy diagram for the initiation reaction. Values in the figure are energies in kcal mol^{-1} relative to **2**+HMI. Those in parentheses are activation energies for each step.

such as **7a**(*R*) and **7a**(*S*) in which the enolate oxygens coordinate to Zn^{2+}. A barrier height for the intra-conversion between **6a** and **7a**(*S*) turned out to be 8.8 kcal mol^{-1}. The energy difference between **6a** and **7a**(*S*) turned out to be only 1.2 kcal mol^{-1} at the B3LYP/LANL2DZ level of theory while they are stable by more than ca. 20 kcal mol^{-1} in comparison with the products of Path A such as **4a**(TS,*R*).

According to barrier heights calculated for both the mechanisms, Path A via the coordination of HMI to the catalyst is preferred to Path B.

3.2. Effects of a bulky substituent in the chiral ligand and of solvent

The IMOMO calculations were performed for complexes with a diphenyl methyl group in the chiral ligand to investigate the steric effect for the initiation reaction. To examine the relation on geometry between the methyl group and the pyrrolidine ring of the chiral ligand, a conformation search of **2** was performed.[13] It was confirmed that the methyl group in the chiral carbon of **1S** is closely related to the geometry of the pyrrolidine ring. That is, the methyl group is *anti* to the pyrolidine ring in its most stable geometry of **2b** as shown in Scheme 4. The scheme shows the bottom view of the optimized geometry of the chiral complex **2b**. In this scheme, neither the ethyl group coordinating to Zn^{2+} nor hydrogen atoms is displayed. The stable geometry with the methyl group *syn* to the ring turned out to be less stable by 1.8 kcal mol^{-1} than the *anti* conformer.

Scheme 4 is very suggestive to understand possible routes for the RMI approach to **2** in Path A. When RMI comes

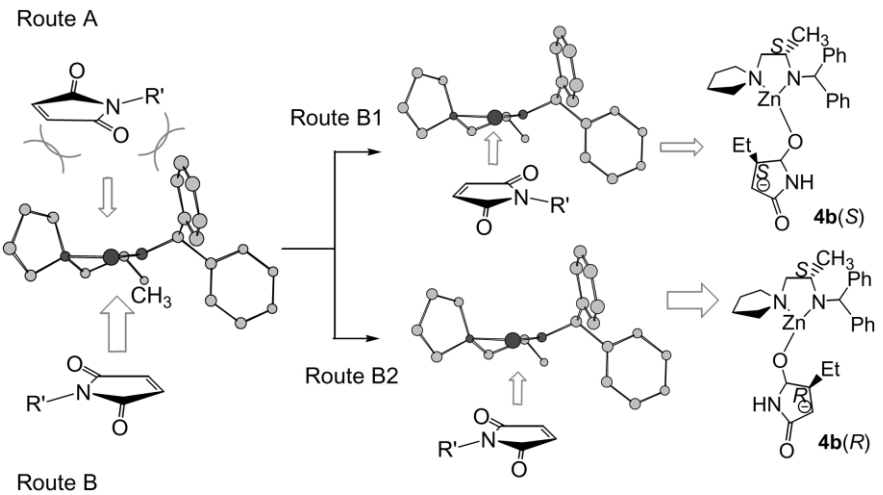

Scheme 4.

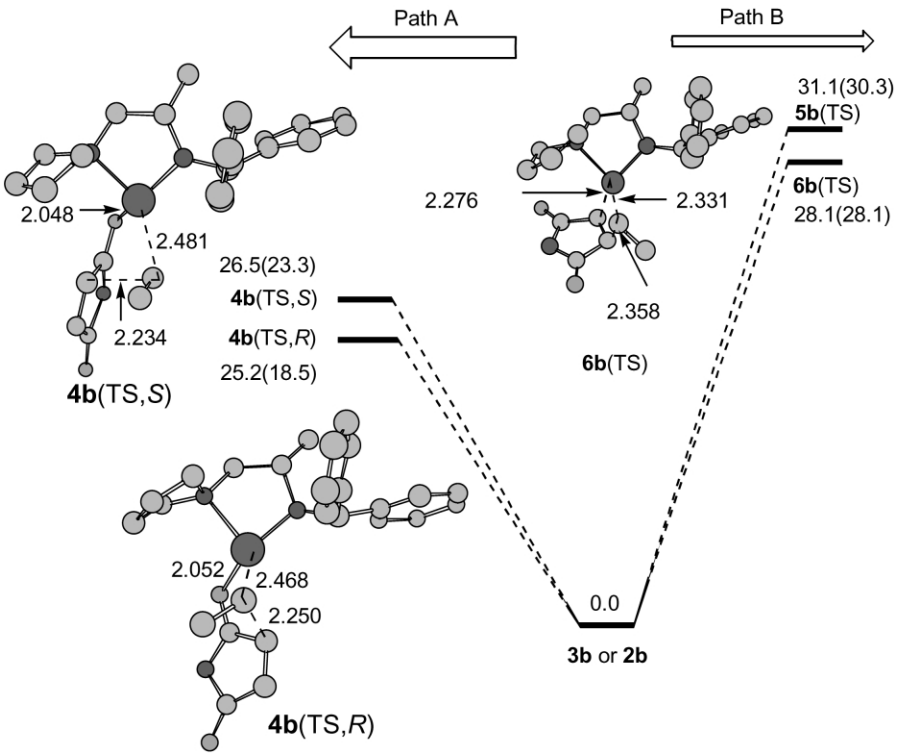

Figure 2. Activation energies of initiation reactions including substituent effects. Values in parentheses are those including solvent effects by using the COSMO method.

close to **2b** via Route A to form **3** (the upper side of the catalyst), the RMI feels steric repulsion between the substituent of RMI and a phenyl group of the chiral ligand. In fact, we could locate no TS structures for the route even though we used HMI as a monomer.

It is not very difficult to realize that the steric repulsion between the RMI and the chiral ligand in Route B (the lower side of the catalyst) is smaller than that in Route A. When the RMI approaches the Zn^{2+} via Route B, there are two possible directions of the substituent of RMI. In one case, the N-substituent directs to one of the phenyl rings of the diphenyl methyl group, Route B1. This approach causes the steric repulsion between the N-substituent and the phenyl group. The reaction with this RMI forms **4b**(*S*). On the other hand, the N-substituent locates close to the pyrrolidine ring of the chiral ligand and this approach results in producing **4b**(*R*), Route B2. In this route, there is little steric effects between the N-substituent and the pyrrolidine ring.

As shown in Figure 2, the energy difference between **4b**(TS,*S*) and **4b**(TS,*R*) is not as large as that expected, i.e. the difference is only 1.3 kcal mol^{-1}. As we calculated the TSs for the HMI, an RMI with a large N-substituent such as a cyclohexyl group is expected to have larger energy difference. However, the calculated activation barriers for Path A ($\sim$25 kcal mol^{-1}) are little higher than those expected from the experiments since the reaction proceeds at 0°C.

In order to estimate the bulk solvent effect for the energy relation among related structures for the polymerization in toluene, energy calculations using the COSMO method[14] were performed. In these calculations, the geometries were the same as those obtained in the vacuum. The activation energy of the path via **4b**(TS,*R*) was calculated to be 18.5 kcal mol^{-1}. The bulk solvent effect reduces the activation energy by 6.7 kcal mol^{-1}. The energy difference between **4b**(TS,*R*) and **4b**(TS,*S*) turned out to be 4.8 kcal mol^{-1} whose value is larger by 3.5 kcal mol^{-1} than that in the vacuum. As activation energies for Path B in toluene are almost the same as those in the vacuum, their absolute values are still larger by more than 10 kcal mol^{-1} than those of Path A.

It means that the initiation reaction proceeds via Path A involving the coordination of HMI to **2b**. While the carbon with the ethyl group in **4**(*S*) possesses the *S* configuration, that in **4**(*R*) has the *R* configuration. Therefore, the major products of the initiation reaction using **2** with **1**(*S*) is **4**(*R*). Further calculations using **2** with **1**(*R*) (**1** with the chiral lingad with the *R* configuration) proved the major products to be **4**(*S*). Therefore, the configuration of the chiral carbon in DPhBP is closely related to the chirality of its five-membered ring in the product of the initiation reaction.

3.3. Plausible mechanisms for the first propagation reaction

Experimental results showed that not the helical structure but the configuration of main chain carbons is mainly responsible for the optical property of the RMI-polymers.[15] As the polymers using the DPhBP catalyst are optically active, their main chains include *threo*-diisotatctic structures. According to the present analysis of the initiation reaction on the model catalyst, the **4**(*R*) is the preferable reactant for successive propagation reactions. It is,

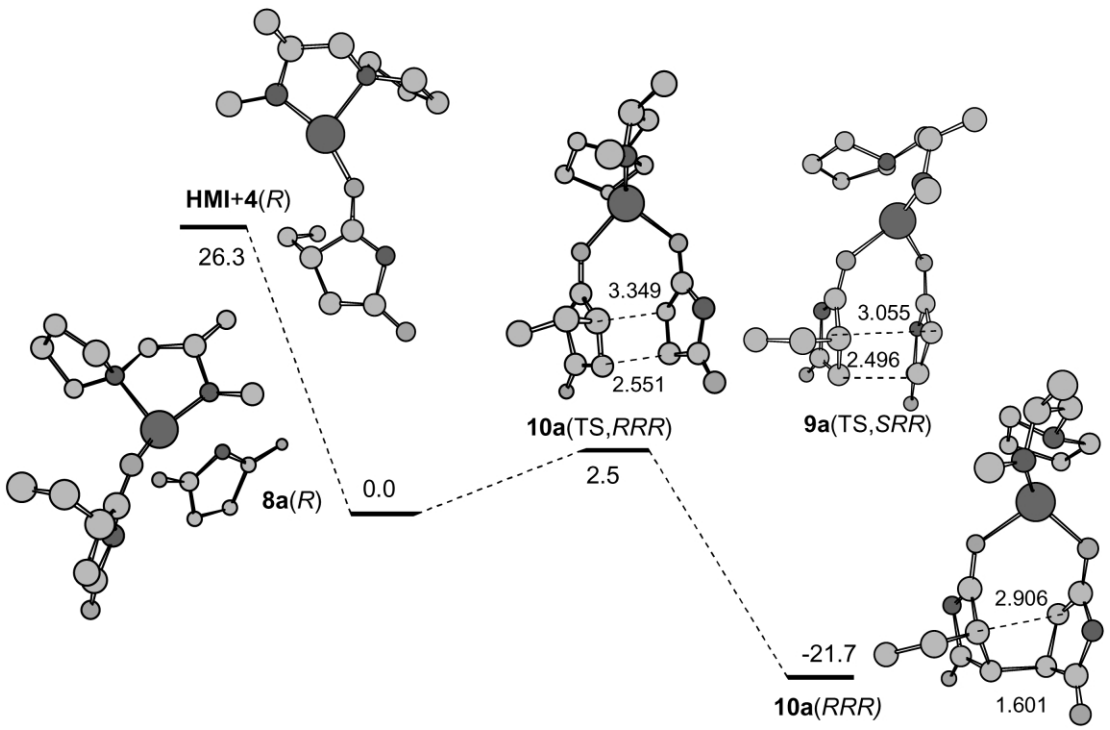

Figure 3. Energy diagram relative to **8**(*R*) for the first propagation reaction. Hydrogen atoms of stable and TS structures in the figure are omitted.

therefore, necessary to investigate why formation of **4**(*R*) triggers the stereospecific polymerization producing continuous *R* configurations in the main chain.

The coordination of the second HMI to **4a**(*R*) produces **8a**(*R*) as shown in Figure 3 and turned out to release stabilization energy by -26.3 kcal mol^{-1} at the B3LYP/LANL2DZ//RHF/LANL2DZ level of theory. This value is much larger than the corresponding value (-8.8 kcal mol^{-1}) of the coordination of HMI to **2a**. Therefore, the propagation reaction proceeds after another monomer coordinates to **4a**(*R*).

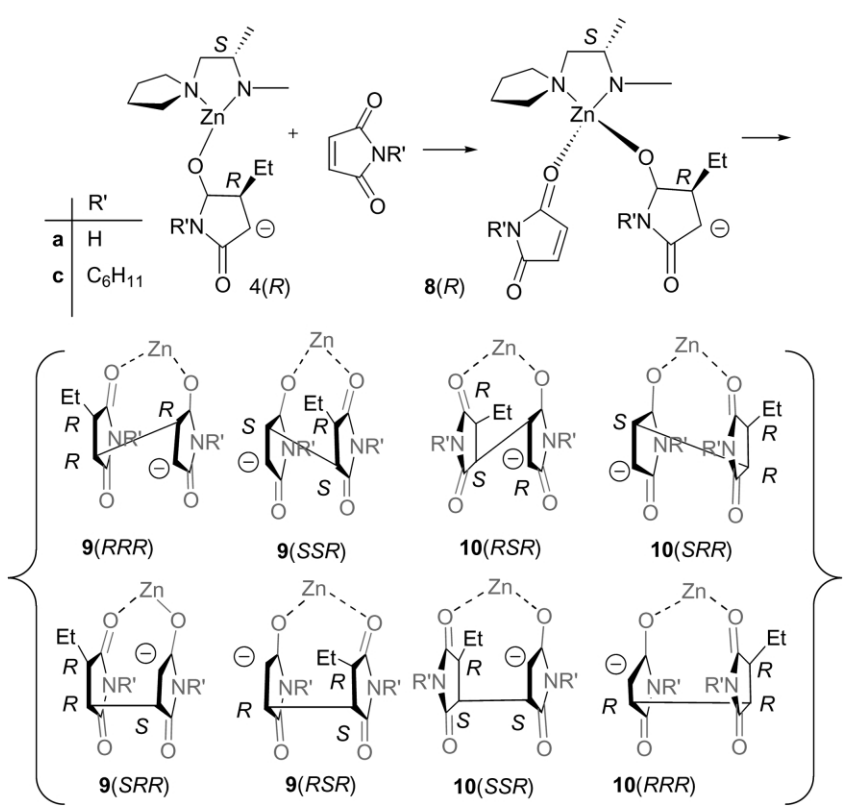

Scheme 5.

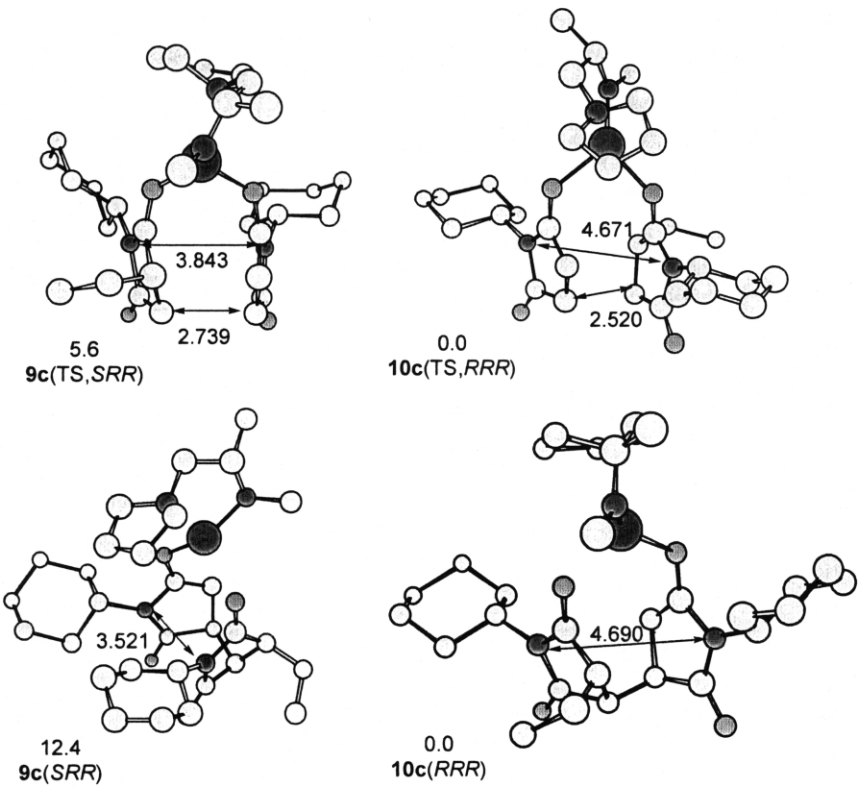

Figure 4. Stable and TS structures of the first growth reactions with the *N*-cyclohexyl substituents. Values in the figure are energies in kcal mol^{-1} relative to **10c**(*RRR*) or **10c**(TS,*RRR*).

It is possible to consider four different geometry on the basis of directions and relative positions of two five-membered rings in **8**(*R*). The anion center can react with one of olefinic carbons in the coordinated RMI. These features on the intermediate geometry yield eight types of products as shown in Scheme 5. We can divide these products to two categories, i.e. one has the geometry with the ethyl group locating inside between the two five-membered rings such as **9**(*SSR*) and the other outside like **10**(*RRR*).[§] It is not much difficult to realize that **9**(*SSR*), **9**(*RSR*), **10**(*RSR*) and **10**(*SSR*) with the former geometry are unlikely to participate in propagation reactions since the ethyl group between the two five-membered rings causes serious steric instability.

In the latter geometry, there are two types of stacking of the two rings. Figure 4 shows products as well as TSs using *N*-cyclohexyl maleimide as a monomer. These structures were optimized at the RHF/LANL2DZ level of theory. As the nitrogen atoms in the polymer moiety of **9c**(*SRR*) almost overlap each other, the N–N distances were calculated to be only 3.521 Å. A repulsive interaction between two cyclohexyl groups also destabilize the product, and then, the stabilization energy due to a C–C bond formation was calculated to be only 10.1 kcal mol^{-1}. On the other hand, the N–N distance in **10c**(*RRR*) was calculated to be 4.690 Å. There is almost no overlapping between the two five-membered rings, i.e. **10c**(*RRR*) is free from the steric repulsion between the two rings. These differences on geometry cause difference in the relative stability between **9c**(*SRR*) and **10c**(*RRR*). Their energy difference was calculated to be as large as 12.4 kcal mol^{-1}. **10**(*RRR*) has an enolate oxygen coordinating to Zn^{2+}, and therefore, this reaction turned out to be exothermic by as large as 21.7 kcal mol^{-1}.

The relative stability among the TSs inherits that among the products. Table 2 summarizes energies relative to **10**(TS,*RRR*) in which all the main chain carbons possess the *R* configuration. Two TSs, **9**(TS,*RRR*) and **10**(TS,*RRR*), produce dimers with three *R* configuration carbons in the main chain. The latter turned out to be the most stable one in the four TSs obtained for the first propagation reactions for both HMI and CHMI. **9a**(TS,*SRR*), in which the two five-membered rings almost overlap each other (Fig. 4), is unstable only by 2.4 kcal mol^{-1} than **10a**(TS,*RRR*) at the B3LYP/LANL2DZ//RHF/LANL2DZ level of theory. The substitution of cyclohexyl groups on the N atoms destabilizes this geometry and **9c**(TS,*SRR*) is less stable by 9.1 kcal mol^{-1} than **10c**(TS,*RRR*) is less stable than even **10c**(TS,*SRR*) by 3.3 kcal mol^{-1}. It is, therefore, likely that the product of the first propagation reaction has the main chain with *RRR* configuration carbons.

Table 2. Energy differences of TSs relative to **10**(TS,*RRR*) for possible mechanisms of the first propagation reaction at the B3LYP/LANL2DZ//RHF/LANL2DZ(RHF/LANL2DZ) level of theory

N-Substituent	HMI (**a**)	CHMI (**c**)
9(TS,*RRR*)	5.6 (6.9)	9.8 (12.7)
9(TS,*SRR*)	2.4 (3.2)	9.1 (10.7)
10(TS,*SRR*)	5.3 (6.3)	5.8 (7.0)
10(TS,*RRR*)	0.0 (0.0)	0.0 (0.0)

[§] The characters in parenthesis designate the configurations of chiral carbons from that adjacent to the anion center in the main chain.

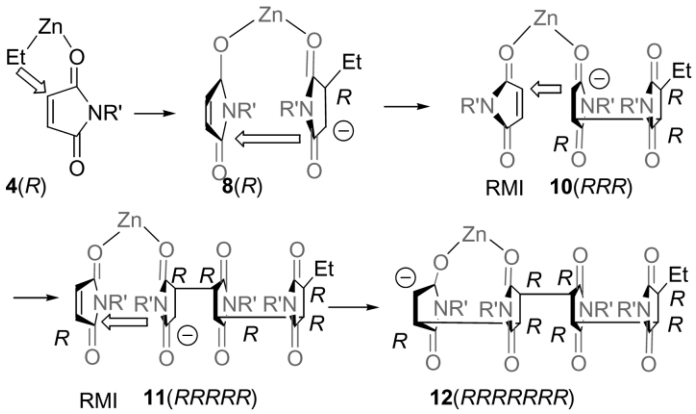

Scheme 6.

3.4. Mechanism of successive propagation reactions

According to the results of present DFT calculations, formation of a new C–C bond proceeds between two nearest carbons seen in **4**(*R*) and **10b**(*RRR*) as shown in Scheme 6. In the initiation reaction, the ethyl group moves to the RMI olefinic carbon close to Zn^{2+} although the enolate oxygen formed does not coordinate to Zn^{2+}. The first propagation reaction yields the product in which the anion center of **8**(*R*) reacts with the coordinated RMI olefinic carbon distant from Zn^{2+} to form an enolate oxygen coordination to Zn^{2+}. Both the reactions minimizes the steric repulsions in the products as well as the TSs. Scheme 6 also displays a possible product of the second propagation reaction which proceeds to form **11**(*RRRRR*) under the mechanism similar to the initiation reaction. As the mechanism of the third propagation reaction is almost the same as that of the first propagation reaction, **12**(*RRRRRRR*) forms. Both the reactions expect to produce continuous *R* configurations in the polymer main chain.

4. Concluding remarks

In the present study, we investigated the polymerization mechanism of RMI by using the model catalyst of Zn^{2+}–DPhBP. We can summarize the findings of our theoretical study as follows.

(1) As the catalyst **2** has an empty coordination site of Zn^{2+}, the carbonyl oxygen of RMI can coordinate to the metal ion. This effect stabilizes the TS for both the initiation reaction and the propagation reaction.
(2) The configurations of the chiral carbon in the Zn^{2+} catalyst is responsible for the formation of configurations of the main chain carbons in the RMI polymers. That is, polymerization with the *S*-configuration carbon in the chiral ligand produces polymers mainly with the *R*-configuration carbons. This is consistent with the experimental results.
(3) The bulky diphenylmethyl substituent in the chiral ligand is effective to enhance the formation of polymers with only the *R*-configuration carbons because of the steric repulsion between the group and the substituent of RMI monomers in the propagation reaction. It is also confirmed that the bulky substituent on the N atom of the RMI is another factor for obtaining polymers with high $[\alpha]^{25}_{435}$.

References

1. Okamoto, U.; Nakano, T. *Chem. Rev.* **1994**, *94*, 349.
2. Nakano, T.; Okamoto, Y. *Kagaku Sousetu, 'Seimitu Jugo'*; Gakkai Shuppan Center, 1993; pp 129–136.
3. Mukai, K.; Doi, Y. *Kagaku Zoukan, No. 123, Molecular chirality, Kagaku Doujin*, 1993; pp 128–129.
4. Cubbon, R. C. P. *Polymer* **1965**, *6*, 419.
5. (a) Oishi, T.; Yamasaki, H.; Fujimoto, M. *Polym. J.* **1991**, *23*, 795. (b) Oishi, T.; Onimura, K.; Tanaka, K.; Horimoto, W.; Tsutsumi, H. *J. Polym. Sci., Part A: Polym. Chem.* **1999**, *37*, 473. (c) Oishi, T.; Onimura, K.; Sumida, W.; Zhou, H.; Tsutsumi, H. *Polym. J.* **2000**, *32*, 543. (d) Zhou, H.; Onimura, K.; Tsutsumi, H.; Oishi, T. *Polym. J.* **2000**, *32*, 552.
6. (a) Onimura, K.; Tsutsumi, H.; Oishi, T. *Chem. Lett.* **1998**, 791. (b) Onimura, K.; Tsutsumi, H.; Oishi, T. *Macromolecules* **1998**, *31*, 5971–5976.
7. Oishi, T.; Onimura, K.; Isobe, Y.; Tsutsumi, H. *Chem. Lett.* **1999**, 673.
8. (a) Isobe, Y.; Onimura, K.; Tsutumi, M.; Ohishi, T. *Macromolecules* **2001**, *34*, 7617. (b) Isobe, Y.; Onimura, K.; Tsutsumi, H.; Oishi, T. *J. Polym. Sci., Part A: Polym. Chem.* **2001**, *39*, 3556.
9. Ohno, H.; Onimura, K.; Oishi, T.; Hori, K. *J. Comput. Aided Chem.* **2002**, *3*, 107.
10. Frisch, M. J.; Trucks, G. W.; Schlegel, H. B.; Scuseria, G. E.; Robb, M. A.; Cheeseman, J. R.; Zakrzewski, V. G.; Montgomery, J. A., Jr.; Stratmann, R. E.; Burant, J. C.; Dapprich, S.; Millam, J. M.; Daniels, A. D.; Kudin, K. N.; Strain, M. C.; Farkas, O.; Tomasi, J.; Barone, V.; Cossi, M.; Cammi, R.; Mennucci, B.; Pomelli, C.; Adamo, C.; Clifford, S.; Ochterski, J.; Petersson, G. A.; Ayala, P. Y.; Cui, Q.; Morokuma, K.; Malick, D. K.; Rabuck, A. D.; Raghavachari, K.; Foresman, J. B.; Cioslowski, J.; Ortiz, J. V.; Baboul, A. G.; Stefanov, B. B.; Liu, G.; Liashenko, A.; Piskorz, P.; Komaromi, I.; Gomperts, R.; Martin, R. L.; Fox, D. J.; Keith, T.; Al-Laham, M. A.; Peng, C. Y.; Nanayakkara, A.; Challacombe, M.; Gill, P. M. W.; Johnson, B.; Chen, W.; Wong, M. W.; Andres, J. L.; Gonzalez, C.; Head-Gordon, M.;

Replogle, E. S.; Pople, J. A. *Gaussian 98*, *Revision A.9*; Gaussian, Inc.: Pittsburgh, PA, 1998.
11. (a) Dunning, T. H., Jr.; Hay, P. J. *Modern Theoretical Chemistry*, Shaefer, H. F. III, Ed.; Plenum: New York, 1976; Vol. 3, p 1. (b) Hay, P. J.; Wadt, W. R. *J. Chem. Phys.* **1985**, *82*, 270.
12. Humbel, S.; Sieber, S.; Morokuma, K. *J. Chem. Phys.* **1996**, *16*, 1959.
13. The conflex program in CAChe ver. 4.3, Fujitsu, Ltd.
14. (a) Klamt, A.; Schuurmann, G. J. *J. Chem. Soc., Perkin Trans. 2* **1993**, 799. (b) Barone, V.; Cossi, M. *J. Phys. Chem.* **1998**, *A102*, 1998.
15. Oishi, T.; Onimura, K.; Isobe, Y.; Yanagihara, H.; Tsutsumi, H. *J. Polym. Sci., Part A: Polym. Chem.* **2000**, *38*, 310.